DOI: 10.1021/ic100158g

Inorganic Chemistry
Article

Magnetic Properties versus Network Dimensionality of Cerium(III) Octacyanotungstate(V) Compounds

Marcin Kozieł,[†] Robert Pełka,*[,‡] Michał Rams,[§] Wojciech Nitek,[†] and Barbara Sieklucka*[,†]

[†]*Faculty of Chemistry, Jagiellonian University, Ingardena 3, 30-060 Kraków, Poland,* [‡]*H. Niewodniczański Institute of Nuclear Physics PAN, Radzikowskiego 152, 31-342 Kraków, Poland, and* [§]*M. Smoluchowski Institute of Physics, Jagiellonian University, Reymonta 4, 30-059 Kraków, Poland*

Received January 26, 2010

The reaction of cerium(III) nitrate, sodium octacyanotungstate(V), and 2,2′-bipyrimidine (bpm) under various conditions leads to the formation of three new compounds: ionic $[Ce_2(bpm)(dmf)_6(H_2O)_8][W(CN)_8]_2\cdot 3H_2O$ (**1**; dmf = *N*,*N*-dimethylformamide), tetranuclear molecules $[Ce_2(bpm)(dmso)_8(H_2O)_4][W(CN)_8]_2\cdot 4H_2O$ (**2**; dmso = dimethyl sulfoxide), and a two-dimensional inorganic−organic hybrid coordination polymer $\{[Ce_2(bpm)(dmf)_8(H_2O)_2][W(CN)_8]_2\}_n\cdot 2nH_2O$ (**3**), all of which contain the subunit $[Ce_2(\mu\text{-bpm})]$ within the structure. These systems were characterized by single-crystal X-ray diffractometry, FTIR spectroscopy, and thermogravimetric analysis. Magnetic susceptibility measurements for **1**−**3** were performed on polycrystalline samples of the compounds. Magnetic behavior was interpreted in terms of the ligand-field splitting parameters and the exchange interaction between lanthanide centers and a d-electron spin carrier. The results confirmed the ferromagnetic cyano-mediated {Ce−NC−W} interaction J_{CeW} = 1.7 (**2**) and 1.4(3) cm^{-1} (**3**) compared to the antiferromagnetic {Ce−bpm−Ce} interaction $J_{CeCe} = -1.1$ cm^{-1} (**1** and **2**).

Introduction

Previously, we reported on the complete magnetostructural correlation analysis of two series of isomorphous $Ln^{3+}[W(CN)_8]^{3-}$ compounds, (i) one-dimensional chains $[Ln(terpy)(dmf)_4][W(CN)_8]\cdot 6H_2O$ (Ln = Ce, Pr, Nd, Sm, Eu, Gd, Tb, Dy) and (ii) dinuclear molecules $[Ln(terpy)(dmf)_2(H_2O)_2][W(CN)_8]\cdot 3H_2O$ (Ln = Ho, Er, Yb), along with the ionic system $[Tm(terpy)(dmf)_2(H_2O)_3][W(CN)_8]\cdot 4H_2O\cdot dmf$.[1,2] Our continuous interest in such 4f−5d systems is based on their remarkable topologies and encoded multifunctionality.[3−7]

To date, only several bimetallic $Ln^{III}[M(CN)_8]^{n-}$ (M = Mo, W) and trimetallic 3d−4f−5d assemblies have been reported. There is only one compound based on the diamagnetic building block $[M(CN)_8]^{4-}$ described, three-dimensional $[Ln(mpca)_2(H_2O)(CH_3OH)Ln(H_2O)_6W(CN)_8]\cdot nH_2O$ (Ln = Eu, Nd; Hmpca = 5-methyl-2-pyrazinecarboxylic acid)[8] containing cyano and carboxylato bridges. The materials containing the paramagnetic unit $[M(CN)_8]^{3-}$ (M = Mo, W) include compounds with cyano bridges only. This group of magnetic compounds consists of dinuclear molecules $[Ln(terpy)(dmf)_2(H_2O)_2][W(CN)_8]\cdot 3H_2O$ (Ln = Ho, Er, Yb; terpy = 2,2′:6′,2″-terpyridine),[1] one-dimensional $[Ln(terpy)(dmf)_4][W(CN)_8]\cdot 6H_2O\cdot C_2H_5OH$ (Ln = Ce−Dy),[1,2] $Gd(dmf)_6[W(CN)_8]$,[9] and $[Tb(pzam)_3(H_2O)Mo(CN)_8]\cdot H_2O$ (pzam = pyrazine-2-carboxamide),[10] two-dimensional $Sm(H_2O)_5[W(CN)_8]$[11] and $Ln(H_2O)_5[M(CN)_8]$ (Ln = Eu, Tb, Sm, Gd; M = Mo, W),[12,13] and trimetallic molecules of $[\{L^{Me2}NiLn\}\{W(CN)_8\}]$ (Ln = Gd, Tb, Dy, Ho, Er; L^{Me2} = Schiff base).[14]

*To whom correspondence should be addressed. E-mail: barbara.sieklucka@uj.edu.pl (B.S.), robert.pelka@ifj.edu.pl (R.P.). Fax: +48 12 634 05 15 (B.S.), +48 12 662 84 58 (R.P.).

(1) Przychodzeń, P.; Pełka, R.; Lewiński, K.; Supel, J.; Rams, M.; Tomala, K.; Sieklucka, B. *Inorg. Chem.* **2007**, *46*, 8924–8938.
(2) Przychodzeń, P.; Lewiński, K.; Pełka, R.; Bałanda, M.; Tomala, K.; Sieklucka, B. *Dalton Trans.* **2006**, 625–628.
(3) Huang, Y.-G.; Jiang, F.-L.; Hong, M.-C. *Coord. Chem. Rev.* **2009**, *253*, 2814−2834 and references cited therein.
(4) Hong, M. *Cryst. Growth Des.* **2007**, *7*, 10–14.
(5) Bünzli, J.-C. G.; Piguet, C. *Chem. Soc. Rev.* **2005**, *34*, 1048–1077.
(6) Bünzli, J.-C. G.; Piguet, C. *Chem. Rev.* **2002**, *102*, 1897–1928.
(7) For example, see: Zhao, B.; Chen, X.-Y.; Cheng, P.; Liao, D.-Z.; Yan, S.-P.; Jiang, Z.-H. *J. Am. Chem. Soc.* **2004**, *126*, 15394–15395.
(8) Tanase, S.; Prins, F.; Smits, J. M. M.; de Gelder, R. *CrystEngComm* **2006**, *8*, 863–865.
(9) Ikeda, S.; Hozumi, T.; Hashimoto, K.; Ohkoshi, S.-I. *Dalton Trans.* **2005**, 2120–2123.
(10) Prins, F.; Pasca, E.; Jos de Jongh, L.; Kooijman, H.; Spek, A. L.; Tanase, S. *Angew. Chem., Int. Ed.* **2007**, *46*, 6081–6084.
(11) Hozumi, T.; Ohkoshi, S.-I.; Arimoto, Y.; Seino, H.; Mizobe, Y.; Hashimoto, K. *J. Phys. Chem. B* **2003**, *107*, 11571–11574.
(12) Chelebaeva, E.; Larionova, J.; Guari, Y.; Ferreira, R. A. S.; Carlos, L. D.; Almeida Paz, F. A.; Trifonov, A.; Guérin, C. *Inorg. Chem.* **2008**, *47*, 775–777.
(13) Chelebaeva, E.; Larionova, J.; Guari, Y.; Ferreira, R. A. S.; Carlos, L. D.; Almeida Paz, F. A.; Trifonov, A.; Guérin, C. *Inorg. Chem.* **2009**, *48*, 5983–5995.
(14) Sutter, J.-P.; Dhers, S.; Rajamani, R.; Ramasesha, S.; Costes, J.-P.; Duhayon, C.; Vendier, L. *Inorg. Chem.* **2009**, *48*, 5820–5828.

Published on Web 04/09/2010

Scheme 1

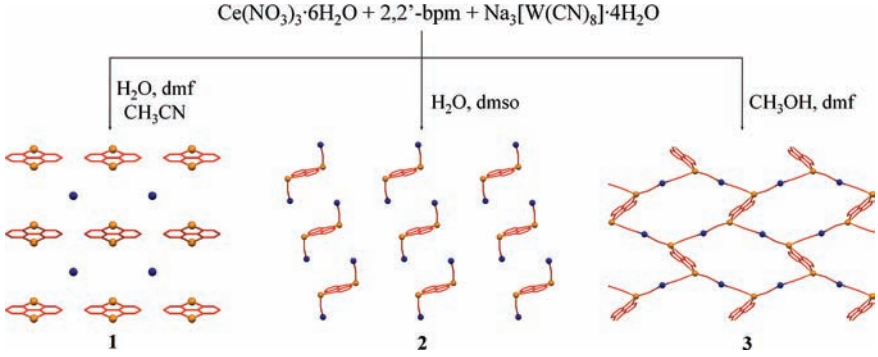

To our knowledge, the construction and characterization of inorganic−organic hybrid materials based on paramagnetic octacyanometallate $[M(CN)_8]^{n-}$ ($M = Mo^V, W^V$) building blocks, 4f metal ions, and organic linkers have not been reported previously. In coordination networks of this type, metal centers give spin and orbital magnetic momentum, cyano bridges provide magnetic coupling, and organic bridges, in addition to magnetic coupling, can supply flexibility and large channels in the structure. Because of the unique nature of Ln ions, such as their large radius, high and variable coordination numbers, and the existence of large spin and considerable orbital moments causing high magnetic anisotropy,[15] the self-assembly of $[M(CN)_8]^{n-}$, 4f metal ions, and organic linkers with novel structures and specific properties offers great challenges and opportunities in terms of controlling their dimensionality and magnetic properties.[16−19]

In the present investigation, we applied bridging 2,2′-bipyrimidine (bpm), the planar polyazine ligand capable of coordinating to two metal centers through four equivalent N atoms, in order to increase the network dimensionality. The bpm ligand was successfully applied in the construction of magnetic materials with 3d[20] and 4f[21,22] ions. The bpm ligand serves also as the molecular antenna in luminescence studies of Ln^{3+}bpm complexes.[23−28]

Here we present crystal engineering of the Ce^{III}bpm-$[W(CN)_8]^{3-}$ system, resulting in ionic $[Ce_2(bpm)(dmf)_6(H_2O)_8][W(CN)_8]_2\cdot 3H_2O$ (**1**), zero-dimensional tetranuclear $[Ce_2(bpm)(dmso)_8(H_2O)_4][W(CN)_8]_2\cdot 4H_2O$ (**2**) and two-dimensional layer $\{[Ce_2(bpm)(dmf)_8(H_2O)_2][W(CN)_8]_2\}_n\cdot 2nH_2O$ (**3**) with a distinctive [Ce(μ-bpm)Ce] motif in their structures (Scheme 1) along with magnetic characterization. The previously introduced method of calculation of the ligand-field (LF) splitting parameters and the exchange interaction between lanthanide centers and a d-electron spin carrier[1,2] allowed for estimation of the LF parameters and coupling constants for each system.

Experimental Section

Materials and Methods. All basic chemicals and solvents of reagent grade were purchased from commercial sources and used as received. $Na_3[W(CN)_8]\cdot 4H_2O$ was prepared according to literature procedures[29] and recrystallized from methanol. All syntheses were performed in the dark and at room temperature to avoid reduction of $[W(CN)_8]^{3-}$.

Synthesis of $[Ce_2(bpm)(dmf)_6(H_2O)_8][W(CN)_8]_2\cdot 3H_2O$ (1). To a solution of $Ce(NO_3)_3\cdot 6H_2O$ (0.13 g, 0.3 mmol) and $Na_3[W(CN)_8]\cdot 4H_2O$ (0.16 g, 0.3 mmol) in water (1 mL) was added a solution of bpm (0.024 g, 0.15 mmol) in *N*,*N*-dimethylformamide (dmf; 0.5 mL) and acetonitrile (1 mL). On the top of the resulting yellow mixture, acetonitrile (2 mL) was carefully layered, avoiding mixing of the two liquids. The yellow crystals formed after 2 days were washed with a small amount of ice-cold water and dried in air. Yield: 0.122 g, 44%. Elem anal. Calcd for $C_{42}H_{70}Ce_2N_{26}O_{17}W_2$: C, 27.13; H, 3.80; N, 19.59. Found: C, 27.11; H, 3.55; N, 19.35. FTIR spectrum in the ν_{CN} region (cm^{-1}): 2164 (m), 2152 (m).

Synthesis of $Ce_2(bpm)(dmso)_8(H_2O)_4[W(CN)_8]_2\cdot 4H_2O$ (2). To a solution of $Ce(NO_3)_3\cdot 6H_2O$ (0.13 g, 0.3 mmol) and $Na_3[W(CN)_8]\cdot 4H_2O$ (0.16 g, 0.3 mmol) in water (1 mL) was added a solution of 2,2′-bipyrimidine (bpm; 0.024 g, 0.15 mmol) in dimethyl sulfoxide (dmso; 0.5 mL). After 1 day, the green precipitate was filtered from the yellow solution and dissolved in water (4 mL). On the top of the resulting yellow solution, ethanol (2 mL) was carefully added, avoiding mixing of the two liquids. The green crystals obtained after 4 days were washed with a small amount of ice-cold water and dried in air. Yield: 0.048 g, 16%. Elem anal. Calcd for $C_{40}H_{70}Ce_2N_{20}O_{16}S_8W_2$: C, 24.12; H, 3.54; N, 14.07. Found: C, 23.85; H, 3.36; N, 14.21. FTIR spectrum in the ν_{CN} region (cm^{-1}): 2166 (m), 2153 (m).

Synthesis of $\{Ce_2(bpm)(dmf)_8(H_2O)_2[W(CN)_8]_2\}_n\cdot 2nH_2O$ (3). To a solution of $Ce(NO_3)_3\cdot 6H_2O$ (0.13 g, 0.3 mmol) in methanol (2 mL) was added a solution of bpm (0.024 g, 0.15 mmol) in methanol (1.5 mL) and dmf (1 mL). To this mixture was added dropwise with intensive stirring a solution of $Na_3[W(CN)_8]\cdot 4H_2O$ (0.16 g, 0.3 mmol) in methanol (2 mL). After 10 min, white needles of the byproduct were filtered and the crimson solution was left in a dry place for slow evaporation.

(15) Abragam, A.; Bleaney, B. *Electron Paramagnetic Resonance of Transition Ions*; Clarendon Press: Oxford, U.K., 1970.
(16) Sessoli, R.; Powell, A. K. *Coord. Chem. Rev.* **2009**, *253*, 2328−2341 and references cited therein.
(17) Ishikawa, N. *Polyhedron* **2007**, *26*, 2147–2153.
(18) Plečnik, C. E.; Liu, S.; Shore, S. G. *Acc. Chem. Res.* **2003**, *36*, 499–508.
(19) Benelli, C.; Gatteschi, D. *Chem. Rev.* **2002**, *102*, 2369–2387.
(20) Toma, L. M.; Lescouëzec, R.; Pasán, J.; Ruiz-Perez, C.; Vaissermann, J.; Cano, J.; Carrasco, R.; Wernsdorfer, W.; Lloret, F.; Julve, M. *J. Am. Chem. Soc.* **2006**, *128*, 4842–4853.
(21) Ma, B.-Q.; Gao, S.; Su, G.; Xu, G.-X. *Angew. Chem., Int. Ed.* **2001**, *40*, 434–437.
(22) Znovjyak, K. O.; Moroz, O. V.; Ovchynnikov, V. A.; Sliva, T. Y.; Shishkina, S. V.; Amirkhanov, V. M. *Polyhedron* **2009**, *28*, 3731–3738.
(23) Zucchi, G.; Maury, O.; Thuéry, P.; Gumy, F.; Bünzli, J.-C. G.; Ephritikhine, M. *Chem.—Eur. J.* **2009**, *15*, 9686–9696.
(24) Bekiari, V.; Thiakou, K. A.; Raptopoulou, C. P.; Perlepes, S. P.; Lianos, P. *J. Lumin.* **2008**, *128*, 481–488.
(25) Fratini, A.; Richards, G.; Larder, E.; Swavey, S. *Inorg. Chem.* **2008**, *47*, 1030–1036.
(26) Zucchi, G.; Maury, O.; Thuéry, P.; Ephritikhine, M. *Inorg. Chem.* **2008**, *47*, 10398–10406.
(27) Fratini, A.; Swavey, S. *Inorg. Chem. Commun.* **2007**, *10*, 636–638.
(28) Swavey, S.; Krause, J. A.; Collins, D.; D'Cunha, D.; Fratini, A. *Polyhedron* **2008**, *27*, 1061–1069.
(29) Samotus, A. *Polym. J. Chem.* **1973**, *47*, 265.

After 1 day, the crimson crystals were filtered and dried in air. Yield: 0.159 g, 56%. Elem anal. Calcd for $C_{48}H_{70}Ce_2N_{28}O_{12}W_2$: C, 30.68; H, 3.75; N, 20.87. Found: C, 30.86; H, 3.63; N, 20.63. FTIR spectrum in the ν_{CN} region (cm^{-1}): 2173 (m), 2148 (m).

Physical Measurements. Elemental analyses were performed on a EuroEA EuroVector elemental analyzer. IR spectra were measured between 4000 and 400 cm^{-1} on a Bruker EQUINOX 55 spectrometer in KBr pellets. Thermogravimetric analysis (TGA) data in the temperature range 25−400 °C were collected on a Mettler Toledo TGA/SDTA 851e microthermogravimeter equipped with QMS Thermostar GSD 300 T Balzers at a heating rate of 5 °C·min^{-1} in an argon atmosphere. Magnetic susceptibility measurements were carried out upon cooling in a constant magnetic field of 1 kOe over the temperature range 2−300 K using a Quantum Design SQUID (superconducting quantum interference device) magnetometer. The magnetic susceptibility data were corrected for the diamagnetic contribution using Pascal's constants.[30] Isothermal magnetization curves in the field up to 50 kOe were measured at T = 1.8 K.

X-ray Crystallographic Data Processing. The crystal structures of **1**−**3** were determined from the single-crystal X-ray diffraction data collected at 293(2) K with a Nonius Kappa CCD diffractometer with graphite-monochromated Mo Kα radiation (λ = 0.710 73 Å). For cell refinements and data reduction, the *DENZO* and *SCALEPACK*[31] programs were used. For structure solution and refinement, *SIR-97*[32] and *SHELXL-97*[33] programs with the *WinGX*[34] graphical user interface were used. The non-H atoms, with exceptions of disordered C41 and C42 atoms in **2**, were refined anisotropically using weighted full-matrix least squares on F^2. All H atoms joined to C atoms of the organic component were positioned with an idealized geometry and refined using a riding model with U_{iso}(H) fixed at 1.2U_{eq}(C) for aromatic C−H and 1.5U_{eq}(C) for the methyl groups. H atoms joined to O atoms coordinating Ce ions were found from the difference Fourier map. The positions of H atoms of crystal water molecules are inaccessible. The geometry of $[W(CN)_8]^{3-}$ ions has been established by continuous shape measures (CShM) analysis, following the ideas of Alvarez and co-workers.[35−38]

Results and Discussion

Structural Description of 1. A view of the building units of **1** is presented in Figure 1a, and the crystal packing is shown in Figure 1b. The structural parameters for **1** are listed in Table 1. The crystal structure of **1** consists of cerium complex cations $[Ce_2(\mu\text{-bpm})(dmf)_6(H_2O)_8]^{6+}$, $[W(CN)_8]^{3-}$ anions, and slightly delocalized water molecules (Figure 1). The cerium complex consists of two Ce^{III} cations bridged by the bpm ligand with a Ce···Ce

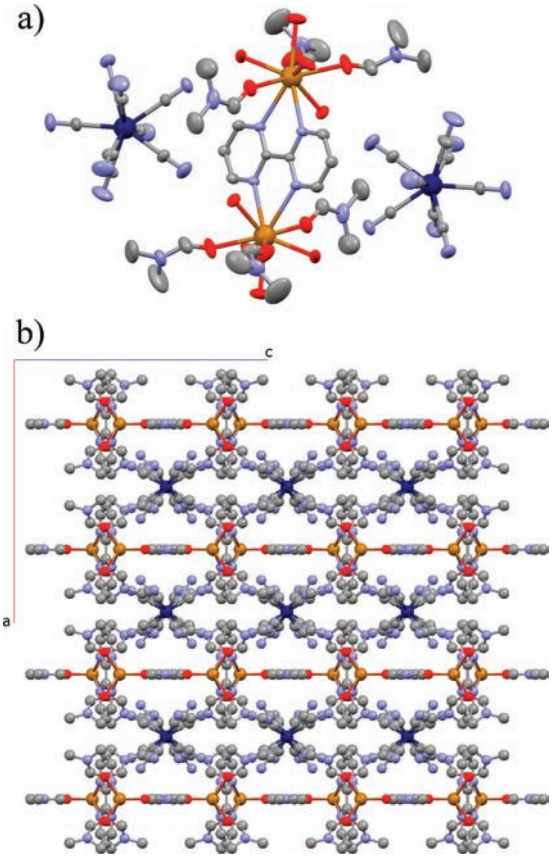

Figure 1. (a) View of the building units of **1** (H atoms and noncoordinated water molecules omitted for clarity; metal ions as spheres, other atoms as ellipsoids 50%). (b) Crystal packing in **1**, a view along the *b* direction (H atoms and all water molecules omitted for clarity).

distance of 7.11 Å and a bite angle N−Ce−N of 59.7°, typical for early lanthanides.[21,22,39,40] Each of the cerium centers of coordination number CN = 9 (Figure S1 in the Supporting Information) coordinates also three molecules of dmf and four water molecules. The coordination sphere of W^V (CN = 8) has an intermediate shape between dodecahedron and square antiprism; the CShM and other shape parameters are presented in Table 2. Average bond lengths W−C (2.156 Å) and C−N (1.143 Å) and angles W−C−N (178°) are in the ranges typical for octacyanometalates.[41,42] Selected bonds lengths and angles are presented in Table 3. The closest distance between Ce and W atoms equals 7.64 Å. There is a small disorder in the structure, resulting in elongation of the thermal ellipsoids of the dmf atoms.

Structural Description of 2. The asymmetric unit of **2** is presented in Figure S2 in the Supporting Information, and the crystal packing of **2** is presented in Figure 2. The structural parameters for **2** are listed in Table 1. The crystal structure of **2** consists of neutral four-centric molecules containing two Ce^{III} ions and two octacyanotungstate(V) building units as well as water molecules (Figure 2). The coordination sphere of Ce atoms

(30) Kahn, O. *Molecular Magnetism*; VCH: New York, 1993.
(31) Otwinowski, Z.; Minor, W. Macromolecular Crystallography. In *Methods in Enzymology*; Carter, C. W., Jr., Sweet, R. M., Eds.; Academic Press: New York, 1997; Vol. *276*, Part A, pp 307−326.
(32) Altomare, A.; Burla, M. C.; Camalli, M.; Cascarano, G. L.; Giacovazzo, C.; Guagliardi, A.; Moliterni, A. G. G.; Polidori, G.; Spagna, R. *J. Appl. Crystallogr.* **1999**, *32*, 115–119.
(33) Sheldrick, G. M. *Acta Crystallogr.* **2008**, *A64*, 112–122.
(34) Farrugia, L. J. *J. Appl. Crystallogr.* **1999**, *32*, 837–838.
(35) Alvarez, S.; Alemany, P.; Casanova, D.; Cirera, J.; Llunell, M.; Avnir, D. *Coord. Chem. Rev.* **2005**, *249*, 1693–1708.
(36) Casanova, D.; Cirera, J.; Llunell, M.; Alemany, P.; Avnir, D.; Alvarez, S. *J. Am. Chem. Soc.* **2004**, *126*, 1755–1763.
(37) Casanova, D.; Llunell, M.; Alemany, P.; Alvarez, S. *Chem.—Eur. J.* **2005**, *11*, 1479–1494.
(38) Llunell, M.; Casanova, D.; Cirera, J.; Bofill, J. M.; Alemany, P.; Alvarez, S.; Pinsky, M.; Avnir, D. *SHAPE*, version 1.1b; University of Barcelona: Barcelona, Spain, **2005**.
(39) Visinescu, D.; Toma, L. M.; Fabelo, O.; Ruiz-Pérez, C.; Lloret, F.; Julve, M. *Polyhedron* **2009**, *28*, 851–859.
(40) Baker, M. H.; Dorweiler, J. D.; Ley, A. N.; Pike, R. D.; Berry, S. M. *Polyhedron* **2009**, *28*, 188–194.
(41) Sieklucka, B.; Podgajny, R.; Przychodzeń, P.; Korzeniak, T. *Coord. Chem. Rev.* **2005**, *249*, 2203–2221.
(42) Przychodzeń, P.; Korzeniak, T.; Podgajny, R.; Sieklucka, B. *Coord. Chem. Rev.* **2006**, *250*, 2234–2260.

Table 1. Crystallographic Data for **1**−**3**

compound	**1**	**2**	**3**
formula	$C_{42}H_{70}Ce_2N_{26}O_{17}W_2$	$C_{40}H_{70}Ce_2N_{20}O_{16}S_8W_2$	$C_{48}H_{70}Ce_2N_{28}O_{12}W_2$
fw	1859.1	1991.5	1879.2
cryst syst	orthorhombic	triclinic	monoclinic
space group	*Cmca*	$P\bar{1}$	$P2_1/c$
temp/K	293(2)	293(2)	293(2)
a/Å	19.362(5)	10.215(5)	10.673(5)
b/Å	19.545(5)	11.218(5)	19.808(5)
c/Å	18.653(5)	16.544(5)	19.284(5)
α/deg	90.000(5)	86.114(5)	90.000(5)
β/deg	90.000(5)	74.056(5)	117.424(16)
γ/deg	90.000(5)	87.544(5)	90.000(5)
V/Å^3	7059(3)	1818.1(13)	3619(2)
Z	4	1	2
cryst size/mm	0.25 × 0.25 × 0.18	0.3 × 0.2 × 0.08	0.28 × 0.25 × 0.18
cryst color	yellow	green	crimson
μ(Mo Kα)/mm^{-1}	4.589	4.679	4.473
parameters	216	409	424
R1 [$I > 2\sigma(I)$]	0.031	0.0417	0.0354
wR2 [$I > 2\sigma(I)$]	0.0713	0.1049	0.0753
S	1.074	1.057	1.081

Table 2. CShM, Minimal Distortion Path Deviation Functions (Δ_i), and the Angular Path Fractions (ϕ) for Molybdenum Centers in **1**−**3**[35−38] (DD = Dodecahedron, SAPR = Square Antiprism)

	1	**2**	**3**
CShM(DD)	0.705	2.235	0.285
CShM(SAPR)	1.106	0.163	2.097
$\theta_{DD-SAPR}$	9.716	9.716	9.716
$\Delta_{DD-SAPR}$	0.117	0.123	0.172
$\phi_{DD\rightarrow SAPR}$	49.6%	88.5%	31.5%
$\phi_{SAPR\rightarrow DD}$	62.1%	23.8%	85.7%
geometry	intermediate between DD and SAPR	slightly distorted SAPR	distorted DD

Table 3. Selected Bonds (in Angstroms) and Angles (in Degrees) for **1**[a]

W1−C1	2.155(3)	C1−N1	1.146(4)
W1−C2	2.158(3)	C2−N2	1.144(4)
W1−C3	2.161(3)	C3−N3	1.140(4)
W1−C4	2.151(3)	C4−N4	1.145(4)
C2−W1−C4′	71.34(11)	C1−W1−C2′	76.97(11)
C2−W1−C2′	71.71(15)	C3−W1−C4′	78.26(13)
C1−W1−C2	75.17(11)	C1−W1−C1′	145.44(16)
C3−W1−C4	75.19(13)	C4−W1−C4′	146.75(16)
Ce2−N32	2.730(2)	N32−C31	1.341(2)
Ce2−O11	2.469(2)	N32−C33	1.342(3)
Ce2−O21	2.508(3)	O11−C12	1.222(4)
Ce2−O4	2.540(3)	C12−N13	1.293(5)
Ce2−O5	2.480(2)	O21−C22	1.223(6)
Ce2−O6	2.559(3)	C22−N23	1.292(6)
N32−Ce2−N32″	59.67(8)	Ce2−N32−C31	122.75(16)
O11−Ce2−O11″	88.43(17)	C31−N32−C33	116.1(2)
O5−Ce2−O6	73.46(7)	Ce2−O11−C12	143.7(3)
O4−Ce2−N32	66.73(8)	Ce2−O21−C22	151.5(4)
O21−Ce2−N32	70.55(9)	avg W1−C−N	178.2(4)

[a] Symmetry operations: ′, $-^3/_2 - x, y, {}^1/_2 - z$; ″, $-1 - x, y, z$.

(CN = 9; Figure S1 in the Supporting Information) consists of two N atoms of bridging bpm (bite angle of 58.0°, characteristic of early lanthanides[21,22,39,40]), one N atom of bridging CN^- (Ce−N distance of 2.663 Å; Ce−N−C angle of 164.6°), four O atoms of dmso, and two water molecules. The coordination sphere of W^V (CN = 8) has the shape of slightly distorted square antiprism; the CShM and other shape parameters are presented in Table 2. Average bond lengths W−C (2.158 Å) and C−N (1.150 Å) and angles W−C−N (178°) are in the ranges typical for octacyanometalates.[41,42] Selected bonds lengths and angles are presented in Table 4. The W···Ce distance

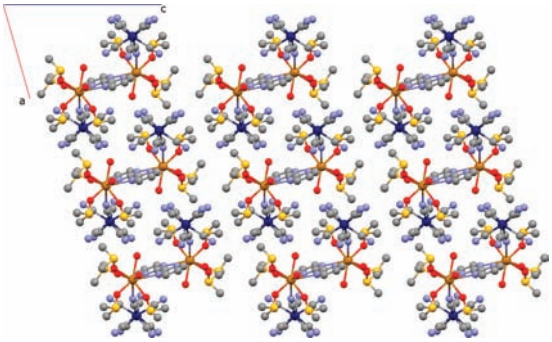

Figure 2. Crystal packing in **2**, a view along the *b* direction. H atoms and noncoordinated water molecules are omitted for clarity.

along the CN bridge equals 5.90 Å, while the intramolecular Ce···Ce distance is equal 7.22 Å. The metric parameters of the CN linkage are close to the parameters reported for $[Ce(terpy)(dmf)_4][W(CN)_8]\cdot 6H_2O\cdot C_2H_5OH$[1] with a slightly smaller Ce−N−C angle (164.6° in **2** in comparison to 169.9° and 168.4° in $[Ce(terpy)(dmf)_4][W(CN)_8]\cdot 6H_2O\cdot C_2H_5OH$). There is significant disorder in the structure concerning solvent molecules, resulting in enlargement of the thermal ellipsoids of the dmso atoms.

Structural Description of 3. The structural parameters for **3** are listed in Table 1. The asymmetric unit of **3** is presented in Figure S3 in the Supporting Information. The crystal structure of **3** consists of cerium complex cations $[Ce_2(\mu\text{-bpm})(dmf)_8(H_2O)_2]$ and $[W(CN)_8]^{3-}$ anions connected with cyano bridges, forming an infinite two-dimensional coordination network (Figure 3). In the coordination sphere of the Ce^{III} ion (CN = 9; Figure S1 in the Supporting Information), there are two N atoms of

Table 4. Selected Bonds (in Angstroms) and Angles (in Degrees) for **2**[a]

W1−C1*	2.150(5)	C1*−N1*	1.160(7)
W1−C2	2.172(5)	C2−N2	1.142(7)
W1−C3	2.151(6)	C3−N3	1.149(8)
W1−C4	2.164(6)	C4−N4	1.141(8)
W1−C5	2.163(5)	C5−N5	1.140(7)
W1−C6	2.164(6)	C6−N6	1.165(8)
W1−C7	2.157(6)	C7−N7	1.128(8)
W1−C8	2.146(6)	C8−N8	1.154(8)
W1−C1*−N1*	176.9(5)		
W1−C2−N2	178.0(5)		
W1−C3−N3	177.0(6)	C1*−N1*−Ce2	164.6(4)
W1−C4−N4	179.4(7)		
W1−C5−N5	179.0(6)	min C2−W1−C3	72.1(2)
W1−C6−N6	179.1(6)	max C3−W1−C5	143.2(2)
W1−C7−N7	177.9(7)		
W1−C8−N8	178.8(6)		
Ce2−N12	2.795(4)		
Ce2−N16′	2.767(4)		
Ce2−N1*	2.663(5)	N12−C11	1.325(6)
Ce2−O2	2.454(4)	N16−C11	1.337(6)
Ce2−O3	2.410(4)	O2−S2	1.519(4)
Ce2−O4	2.531(5)	O3−S3	1.503(5)
Ce2−O5	2.421(4)	O4−S4	1.504(7)
Ce2−O6	2.530(4)	O5−S5	1.500(4)
Ce2−O7	2.505(4)		
N12−Ce2−N16′	58.03(12)		
N1*−Ce2−N12	65.71(15)		
N1*−Ce2−N16′	97.80(15)	Ce2−O2−S2	139.7(2)
O2−Ce2−N16′	66.77(14)	Ce2−O3−S3	141.1(3)
O5−Ce2−N12	69.64(14)	Ce2−O4−S4	128.8(4)
O6−Ce2−N12	71.46(15)	Ce2−O5−S5	144.3(3)
O3−Ce−O4	68.39(17)		
O6−Ce2−O7	78.29(14)		

[a] Symmetry operation: ′, $-1-x, 1-y, 1-z$. Asterisks mark bridging CN ligands.

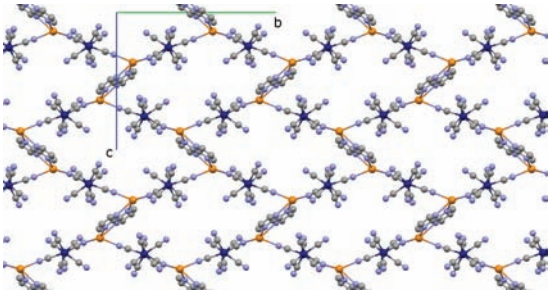

Figure 3. View of the single layer of **3**. H atoms, all water molecules, and dmf ligands are omitted for clarity.

bridging bpm (bite angle of 57.6°; typical for early lanthanides[21,22,39,40]), two N atoms of bridging CN^- (Ce−N distances of 2.618 and 2.637 Å; Ce−N−C angles of 174.8° and 170.5°, respectively), four O atoms of dmf, and one water molecule. The coordination sphere of W^V (CN = 8) has the shape of distorted dodecahedron; the CShM and other shape parameters are presented in Table 2. Average bond lengths W−C (2.160 Å) and C−N (1.144 Å) and angles W−C−N (178.5°) are in the ranges typical for octacyanometalates.[41,42] Selected bonds lengths and angles for **3** are presented in Table 5. The metric parameters of the CN linkage are again close to the parameters reported for $[Ce(terpy)(dmf)_4][W(CN)_8]\cdot 6H_2O\cdot C_2H_5OH$[1] with a slightly greater Ce−N−C angle (174.8° and 170.5° in **3** in comparison to 169.9° and 168.4° in $[Ce(terpy)(dmf)_4][W(CN)_8]\cdot 6H_2O\cdot C_2H_5OH$). The two types of bridging ligands ensure

Table 5. Selected Bonds (in Angstroms) and Angles (in Degrees) for **3**[a]

W1−C1*	2.174(3)	C1*−N1*	1.139(4)
W1−C2	2.157(4)	C2−N2	1.147(5)
W1−C3*	2.165(3)	C3*−N3*	1.151(4)
W1−C4	2.146(4)	C4−N4	1.134(5)
W1−C5	2.158(4)	C5−N5	1.142(5)
W1−C6	2.165(4)	C6−N6	1.144(5)
W1−C7	2.148(4)	C7−N7	1.145(4)
W1−C8	2.166(4)	C8−N8	1.148(5)
W1−C1*−N1*	178.4(3)		
W1−C2−N2	178.5(4)	C1*−N1*−Ce2	174.8(3)
W1−C3*−N3*	178.7(3)	C3*−N3*−Ce2′	170.5(3)
W1−C4−N4	179.0(4)		
W1−C5−N5	178.6(4)	min C3−W1−C4	70.55(14)
W1−C6−N6	178.7(4)	max C4−W1−C5	146.01(15)
W1−C7−N7	176.6(4)	C1*−W1−C3*	134.06(13)
W1−C8−N8	179.2(4)		
Ce2−N52″	2.785(3)	Ce2−O6	2.524(3)
Ce2−N56	2.772(3)		
Ce2−N1*	2.618(3)	N52−C51	1.329(4)
Ce2′−N3*	2.637 (3)	N56−C51	1.331(4)
Ce2−O11	2.419(3)	O11−C12	1.246(5)
Ce2−O21	2.465(3)	O21−C22	1.223(5)
Ce2−O31	2.492(3)	O31−C32	1.243(5)
Ce2−O41	2.463(3)	O41−C42	1.239(4)
N56−Ce2−N52″	57.62(7)		
N1′*−Ce2′−N3*	137.14(10)	Ce2−O11−C12	162.1(3)
N1*−Ce2−N56	79.32(10)	Ce2−O21−C22	135.8(3)
N1*−Ce2−N52″	64.89(9)	Ce2−O31−C32	137.8(3)
O21−Ce2−O31	69.56(11)	Ce2−O41−C42	131.7(3)
O6−Ce2−O41	72.96(10)		

[a] Symmetry operations: ′, $-x, -{}^1/_2+y, {}^1/_2-z$; ″, $-1-x, -y, 1-z$. Asterisks mark bridging CN ligands.

the layered architecture of the crystal lattice. Within the layer (Figure 3), Ce and W ions are connected in alternating fashion, forming bimetallic cyano-bridged chains (W−CN−Ce distances equal to 5.93 Å). These chains are clipped together with bpm (Ce···Ce distance 7.24 Å), forming a waved honeycomb-like net. Each mesh of such a net consists of six Ce ions, four W ions, eight CN bridges, and two bpm bridges. Between the layers, there are slightly delocalized crystallization water molecules. A small disorder in the structure results in enlargement of the thermal ellipsoids of several atoms.

TGA studies show the gradual loss of all water molecules for all compounds in the temperature range 40−138 °C for **1** (10.2% of mass; calcd for $11H_2O$, 10.7%; Figure S4 in the Supporting Information), 40−126 °C for **2** (7.1% of mass; calcd for $8H_2O$, 7.2%; Figure S5 in the Supporting Information), and 70−125 °C for **3** (3.7% of mass; calcd for $4H_2O$, 3.8%; Figure S6 in the Supporting Information). It is apparent that, in the case of two-dimensional compound **3**, the energy barrier for the loss of crystallization water molecules is higher. The top limits for water loss are attributed to the energies of breaking of the coordination H_2O−Ce bonds.

Magnetic Properties. Figures 4−6 show the molar magnetic susceptibility in the form of the χT product against temperature T for powder samples of **1**−**3**, respectively. The corresponding curves display a smooth monotonic decrease with a decrease in the temperature down to 5 K, and then a more rapid change is observed at lower temperatures, which is most apparent for **3**. The values of χT at 300 K are 2.17, 2.44, and 2.15 $cm^3\cdot K\cdot mol^{-1}$ for **1**−**3**, respectively, which

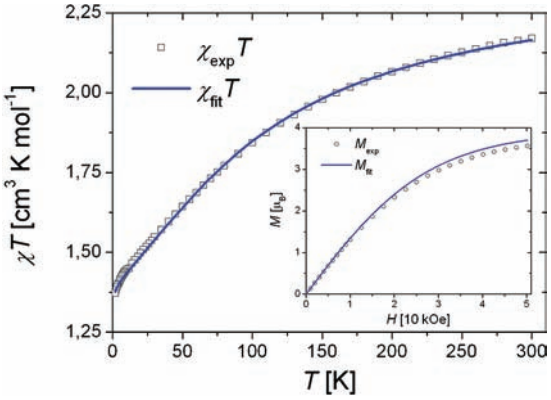

Figure 4. Temperature dependence of χT for **1**. Inset: Isothermal magnetization at $T = 1.8$ K. Solid lines show the best-fit curves.

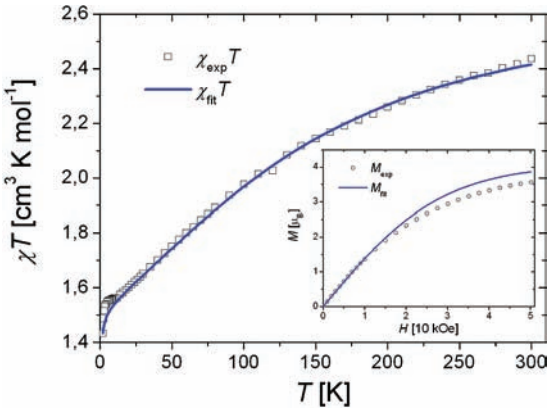

Figure 5. Temperature dependence of χT for **2**. Inset: Isothermal magnetization at $T = 1.8$ K. Solid lines show the best-fit curves.

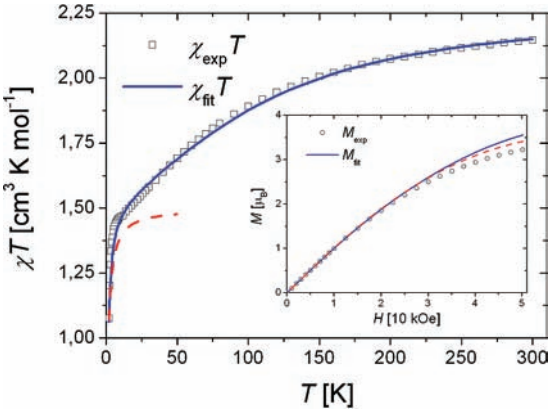

Figure 6. Temperature dependence of χT for **3**. Inset: Isothermal magnetization at $T = 1.8$ K. Solid lines show the best-fit curves. Dashed lines show the results of the eight-center grid model.

are comparable to 2.36 $cm^3 \cdot K \cdot mol^{-1}$ comprising the free-ion contributions from two W^V ions ($S_W = {}^1/_2$; $g_W = 2$) and two Ce^{III} ions ($J = {}^5/_2$; $g_J = {}^6/_7$). In the insets of Figures 4−6, the experimental data for the field dependence of the magnetization at $T = 1.8$ K are shown. The corresponding curves display a monotonic increase with an increasing value of the magnetic field and reach, at $H = 50$ kOe, the values of 3.56, 3.56, and 3.22 $N\beta$ for **1**−**3**, respectively. These are significantly lower than the value of 6.02 $N\beta$ expected on the basis of the free-ion approximation calculated at the same values of temperature and external magnetic field. No significant features were observed in the alternating-current susceptibility measured down to 1.8 K, which indicates no magnetic ordering in this temperature range. The overall magnetic behavior of **1**−**3** can be ascribed to the LF, which splits the ground-state multiplet of the Ce^{III} ion, affecting its magnetic moment. This is the main mechanism responsible for χT variation above 5 K. At lower temperatures, the intramolecular exchange interaction comes into play. Quantitative analysis is presented in the next section.

Determination of the LF Parameters in the Cerium Complexes

General Procedures. The f electrons in the majority of lanthanide complexes are considered to have properties close to those of isolated ions. The energies of the ground- and excited-state multiplets are determined by the spin−orbit coupling in which the total angular momentum J is a good quantum number. The fine structure of the spectral bands detected in the region from near-IR to UV is ascribed to the LF splitting of the ground- and excited-state multiplets. Many studies devoted to the multiplet structures of lanthanide f systems include only the cases for which sharp emission or absorption bands or both were available (see, e.g., ref 43−50). Another approach that can yield some information on the LF splitting is the output of magnetic measurements, which has been applied in systems containing the Ln ions.[51−57]

Analysis of the LF was crucial for rationalizing the magnetic data of bimetallic Ln_2Cu_2 (Ln = Gd, Dy) compounds[58] as well as Ln[organic radical] species.[52,59] The magnetic studies of a homologous series of complexes of the type Ln−M (Ln = La^{III}, Ce^{III}; M = Fe^{III}, Co^{III}) were

(43) Cybińska, J.; Hölsä, J.; Lastusaari, M.; Legendziewicz, J.; Meyer, G.; Wickleder, C. *J. Alloys Compd.* **2004**, *380*, 27.
(44) Gałdecka, E.; Gałdecki, Z.; Cybińska, J.; Wiglusz, R. J.; Amirkhanov, V.; Legendziewicz, J. *Mol. Phys.* **2003**, *101*, 1015.
(45) Popova, M. N.; Klimin, S. A.; Chukalina, E. P.; Malkin, B. Z.; Levitin, R. Z.; Mill, B. V.; Antic-Fidancev, E. *Phys. Rev. B* **2003**, *68*, 155103.
(46) Oczko, G.; Legendziewicz, J.; Wickleder, M. S.; Meyer, G. *J. Alloys Compd.* **2002**, *341*, 255.
(47) Cybińska, J.; Sokolnicki, J.; Legendziewicz, J.; Meyer, G. *J. Alloys Compd.* **2002**, *341*, 115.
(48) Malta, O. L.; Legendziewicz, J.; Huskowska, E.; Turowska-Tyrk, I.; Albuquerque, R. Q.; de Mello Donegá, C.; de Silva, F. R. G. *J. Alloys Compd.* **2001**, *323*−*324*, 654.
(49) Legendziewicz, J.; Borzechowska, M.; Oczko, G.; Meyer, G. *New J. Chem.* **1999**, *24*, 53.
(50) Legendziewicz, J.; Borzechowska, M.; Oczko, G.; Mroziński, J. *Spectrochim. Acta, Part A* **1998**, *54*, 2197.
(51) Sutter, J.-P.; Kahn, M. L.; Golhen, S.; Ouahab, L.; Kahn, O. *Chem.—Eur. J.* **1998**, *4*, 571.
(52) Benelli, C.; Caneschi, A.; Gatteschi, D.; Pardi, L.; Rey, P.; Shum, D. P.; Carlin, R. L. *Inorg. Chem.* **1989**, *28*, 272.
(53) Benelli, C.; Caneschi, A.; Gatteschi, D.; Pardi, L.; Rey, P. *Inorg. Chem.* **1990**, *29*, 4223.
(54) Benelli, C.; Caneschi, A.; Gatteschi, D.; Pardi, L. *Inorg. Chem.* **1992**, *31*, 741.
(55) Bencini, A.; Benelli, C.; Caneschi, A.; Carlin, R. L.; Dei, A.; Gatteschi, D. *J. Am. Chem. Soc.* **1985**, *107*, 8128.
(56) Kahn, M. L.; Sutter, J.-P.; Golhen, S.; Guionneau, P.; Ouahab, L.; Kahn, O.; Chasseau, D. *J. Am. Chem. Soc.* **2000**, *122*, 3413.
(57) Figuerola, A.; Diaz, C.; Ribas, J.; Tangoulis, V.; Granell, J.; Lloret, F.; Mahia, J.; Maestro, M. *Inorg. Chem.* **2003**, *42*, 641.
(58) Benelli, C.; Caneschi, A.; Gatteschi, D.; Guillou, O.; Pardi, L. *J. Magn. Magn. Mater.* **1990**, *83*, 522.
(59) Kahn, M. L.; Ballou, R.; Porcher, P.; Kahn, O.; Sutter, J.-P. *Chem.—Eur. J.* **2002**, *8*, 525.

complemented also by the electron paramagnetic resonance spectra of the constituent ions, which allowed for insight into the anisotropy of the exchange couplings.[60,61] Finally, the approach based solely on magnetic data and using a single set of LF parameters of Ishikawa and coworkers[62−64] showed reproduction of the magnetic properties for isostructural lanthanide-based double-decker complexes. A similar approach was already applied by us in the analysis of a series of compounds comprising the lanthanide species, octacyanotungstate, and the dmf ligand.[1]

The approach depends crucially on the coordination number (CN) of the Ln ion. Crystallographic analysis of compounds **1**−**3** revealed that, in all three cases, CN = 9 and the coordination geometry can be regarded either as a distorted monocapped square antiprism (MSAP, C_{4v}) or a tricapped trigonal prism (TTP, D_{3h}; Figure S1 in the Supporting Information). The structure of compound **1** consists of exchange-coupled dinuclear units formed by Ce^{III} ions and a decoupled pair of W^{V} ions. The structural unit of compound **2** is the exchange-coupled four-center unit $W^{V}-Ce^{III}-Ce^{III}-W^{V}$, whereas in compound **3**, alternating chains of Ce^{III} and W^{V} ions are transversely linked through the bpm ligand, forming two-dimensional sheets. The total angular momentum of the ground state in the trivalent Ce ion takes the minimal value, i.e., $J = |L - S|$ (for electronic configuration f^1) in the Russell−Saunders coupling scheme, i.e., $J = {}^5/_2$. The simulations were carried out using the $2J + 1$ sublevels of the ground-state multiplet in each cerium system.

The total Hamiltonian pertinent to the present systems under an external magnetic field is $H_T = H_Z + H_{LF} + H_{EX}$. The first term accounts for the Zeeman effect. For one Ce^{III} ion and one W^{V} ion, it reads

$$H_Z = \beta(g_J\mathbf{J} + g_W\mathbf{S}_W)\cdot\mathbf{H}$$

where β is the Bohr magneton and $\mathbf{H}$ denotes the external magnetic field. The total magnetic moment operator $\boldsymbol{\mu} = -\beta(g_J\mathbf{J} + g_W\mathbf{S}_W)$ is used in the $|J,J_Z\rangle$ representation in its lanthanide part. $\mathbf{S}_W$ denotes the half spin operator of the tungsten center. The value of g_W is fixed at 2.0, whereas g_J was varied during the fitting procedure. The second term corresponds to the LF interaction, which is expressed in the framework of the extended operator equivalent approach[15,65,66] and is written as

$$H_{LF} = \sum_{2,4,6}\sum_{q=-k}^{k} A_k^q\langle r^k\rangle\langle J\|\alpha_k\|J\rangle O_k^q$$

The coefficients $A_k^q\langle r^k\rangle$ are the parameters to be determined. O_k^q are the Stevens operator equivalents and are polynomials of the total angular momentum operators J_Z, J_+, and J_- (cf. Table S1 in the Supporting Information). Coefficients $\langle J\|\alpha_k\|J\rangle$ relate the angular momentum operators to the potential operators and depend on the ion and the coupling scheme assumed (e.g., $L - S$ or intermediate). Their values are tabulated[66] for all Ln ions in the $L - S$ scheme. The last component of the total Hamiltonian H_{EX} is to account for the exchange coupling between the ions. The coupling should be taken between the corresponding spin operators. The spin operator $\mathbf{S}$ of the lanthanide center can be projected onto the total angular momentum operator $\mathbf{J}$. Equations $\mathbf{L} + \mathbf{S} = \mathbf{J}$ and $\mathbf{L} + 2\mathbf{S} = g_J\mathbf{J}$ imply that this projection is $\mathbf{S} = (g_J - 1)\mathbf{J}$. We further assume that the exchange coupling between the W^{V} and Ce^{III} ions and the Ce^{III} and Ce^{III} ions is isotropic; hence, H_{EX} reads

$$H_{EX} = -J_{CeW}(g_J - 1)(\mathbf{J}_{Ce1}\cdot\mathbf{S}_{W1} + \mathbf{J}_{Ce2}\cdot\mathbf{S}_{W2}) - J_{CeCe}(g_J - 1)^2\mathbf{J}_{Ce1}\cdot\mathbf{J}_{Ce2} \quad (1)$$

The above simplifying assumption does not exclude the anisotropy of exchange interactions in the ground state, which will be demonstrated to be inherited from the anisotropy of the corresponding spectroscopic factor. However, we do not introduce an antisymmetric exchange term,[61,67−69] which would be very unreliable to estimate because of the lack of detailed spectroscopic information.

By diagonalization of the total Hamiltonian H_T, a full set of eigenvalues and eigenfunctions is determined and the magnetic molar susceptibility together with the isothermal magnetization are calculated. This is performed using the generalized van Vleck formalism

$$\chi = \frac{N}{3k_BTZ_0}\sum_{n,i}\left[\sum_j |\langle\varphi_{n,i}|\mu|\varphi_{n,j}\rangle|^2 - 2k_BT\sum_{j,m\neq n}\frac{|\langle\varphi_{n,i}|\mu|\varphi_{m,j}\rangle|^2}{E_n - E_m}\right]\exp\left(-\frac{E_n}{k_BT}\right)$$

$$M = \frac{N}{Z_H}\sum_k\langle\psi_k|\mu|\psi_k\rangle\exp\left(-\frac{E_k(\mathbf{H})}{k_BT}\right)$$

where $Z_0 = \sum_n d_n\exp(-E_n/k_BT)$ and $Z_H = \sum_k\exp(-E_k(\mathbf{H})/k_BT)$. Here $\varphi_{n,i}$ denote the d_n-fold degenerate eigenfunctions with energy E_n in the absence of a magnetic field, whereas the eigensystem $\{\psi_k, E_k(\mathbf{H})\}$ is calculated assuming the nonzero external magnetic field $\mathbf{H}$. The observed molar magnetic susceptibility of the powder sample is $\bar{\chi} = (\chi_x + \chi_y + \chi_z)/3$, where χ_x, χ_y, and χ_z denote the principal values of the magnetic susceptibility. The molar magnetic moment measured on the powder sample is calculated as a mean over 133 different orientations of the external magnetic field parametrized by the couple of spherical angles (θ, φ). The corresponding points are uniformly distributed in the rectangle $(0, 1) \times (0, 2\pi)$ of the $(\cos\theta, \varphi)$ plane.

Fitting was carried out with the help of a specially designed procedure prepared within the *Mathematica 7.0* environment. Two test functions to be minimized were

(60) Figuerola, A.; Tangoulis, V.; Sanakis, Y. *Chem. Phys.* **2007**, *334*, 204.
(61) Sorace, L.; Sangregorio, C.; Figuerola, A.; Benelli, C.; Gatteschi, D. *Chem.—Eur. J.* **2009**, *15*, 1377–1388.
(62) Ishikawa, N.; Sugita, M.; Okubo, T.; Tanaka, N.; Iino, T.; Kaizu, Y. *Inorg. Chem.* **2003**, *42*, 2440.
(63) Ishikawa, N.; Iino, T; Kaizu, Y. *J. Phys. Chem. A* **2002**, *106*, 9543.
(64) Ishikawa, N.; Iino, T; Kaizu, Y. *J. Am. Chem. Soc.* **2002**, *124*, 11440.
(65) Stevens, K. W. H. *Proc. Phys. Soc., London, Sect. A* **1952**, *65*, 209.
(66) Altshuler, S.; Kozyrev, B. M. *Electron Paramagnetic Resonance in Compounds of Transition Elements*; Nauka: Moscow, 1972; in Russian.
(67) Stevens, K. W. H. *Rev. Mod. Phys.* **1953**, *25*, 166.
(68) Levy, P. M. *Phys. Rev. Lett.* **1968**, *20*, 1366.
(69) Levy, P. M. *Phys. Rev.* **1969**, *177*, 509.

used. The first test function was the relative root-mean-square (rms) deviation from the measured χT values. The second one was extended to include additionally the relative rms deviation from the measured M values. The first test function was used in the first step of the fitting procedure, where the LF parameters and the spectroscopic factor g_J of the Ln ions were relaxed but the exchange coupling constants were fixed at zero value. The extended test function was used in the second step, where the LF parameters were fixed at the values found in the first step and the exchange coupling parameters were relaxed. Because the lanthanide site is expected to be of low symmetry, no initial assumptions can be made as to the parameters. On the other hand, the many-dimensional fits where only powder data are available would be of poor reliability. To overcome that problem, the calculations were performed only with different small trial sets of two or three LF parameters. After that, the best set has been chosen. The trial sets were selected on the basis of those corresponding to the distorted MSAP or TTP geometry. Such a treatment is justified if one looks on the resulting parameter sets as the effective ones. In all three cases, the best fits were obtained using the parameter set including $A_2^0\langle r^2\rangle$, $A_4^0\langle r^4\rangle$, and $A_4^3\langle r^4\rangle$. The realization of the best fit through the inclusion of parameter $A_4^3\langle r^4\rangle$ indicates that the coordination is closer to the TTP geometry. Errors of the parameters were estimated assuming 5% tolerance deviation for the test function.

Results for 1. The ground state arising from the $4f^1$ configuration of the Ce^{III} ion is $^2F_{5/2}$. The dimension of its ground-state subspace is, hence, 6. The expected value of the Landé factor g_J is $^6/_7$ (≈ 0.86). The model system comprises two decoupled W^V centers, and two Ce^{III} centers exchange coupled through the bpm ligand. Therefore, we assume $J_{CeW} = 0$. The best fit to the experimental data was found for the following set of parameters (the LF parameters and the exchange coupling constants are always given in cm^{-1}): $g_J = 0.84(1)$, $J_{CeCe} = -1.1(1)$, $A_2^0\langle r^2\rangle = -897(5)$, $A_4^0\langle r^4\rangle = 42(15)$, and $A_4^3\langle r^4\rangle = -1049(6)$. Figure 4 shows the best-fit curves (solid lines) for the susceptibility and isothermal magnetization. The lowest level is a Kramers doublet, which is a superposition of the $|\pm^1/_2\rangle$ and $|\pm^5/_2\rangle$ substates (Table S2 in the Supporting Information), but the dominant contribution comes from the substates with the lowest value of $|J_z|$ (88.8%). The first excited state comprises the $|\pm^3/_2\rangle$ states, and the highest Kramers doublet is again a superposition of the $|\pm^1/_2\rangle$ and $|\pm^5/_2\rangle$ substates with the dominant contribution from the $|\pm^5/_2\rangle$ substates. The population of the lowest Kramers doublet at $T = 2$ K is practically 100%. It is only at $T = 100$ K that the population of the first excited level (4.6%) stops being negligible. The populations of the successive Kramers doublets at $T = 200$ K are 81%, 17.8%, and 1.2%, respectively. This explains the steady decrease of the χT product upon lowering temperature. The tiny downturn of the χT curve at lowest temperatures is ascribed to the "switching-on" of the antiferromagnetic interaction between the cerium centers. Because the lowest-lying Kramers doublet is well-separated from the excited ones, magnetic properties of **1** in the low-temperature regime can be well described by an effective exchange Hamiltonian of the form

$$H_{EFF1} = -\tilde{S}_{Ce1}\cdot\mathbf{J}_{CeCe}\cdot\tilde{S}_{Ce2}$$

where $\mathbf{J}_{CeCe}$ is a symmetric exchange coupling matrix and $\tilde{S}_{Ce1}$ and $\tilde{S}_{Ce2}$ are the effective spin operators corresponding to the lowest doublet. Both the matrix element equivalence relation $\hat{g}_{Ce}\cdot\tilde{S}_{Ce} = \hat{g}_{Ce}J_{Ce}$ and the Hamiltonian in eq 1 imply that matrix $\mathbf{J}_{CeCe}$ is diagonal in the coordinate system where the corresponding spectroscopic factors are diagonal, and its principal values are given by the formula $J_{CeCei} = (g_{Ce} - 1)^2(g_{Ceii}/g_{Ce})^2 J_{CeCe}$, where $i = x, y, z$. Furthermore, matrix $\mathbf{J}_{CeCe}$ can be split into isotropic and anisotropic parts $\mathbf{J}_{CeCe} = J_{iso}\,\mathrm{diag}(1,1,1) + \mathrm{diag}(D_{xx}, D_{yy}, D_{zz})$, where $\mathrm{diag}(a_1, a_2, a_3)$ denotes the diagonal matrix with elements (a_1, a_2, a_3) on the diagonal. Using the principal values of the spectroscopic tensor (Table S2 in the Supporting Information) and the best-fit values of parameters $\mathbf{J}_{CeCe}$ and g_{Ce}, we find $J_{iso} = -0.104$, $D_{xx} = D_{yy} = -0.051$, and $D_{zz} = 0.101$ (in cm^{-1}). The ratio $J_{CeCez}/J_{CeCex(y)} = 0.02$ indicates an XXZ anisotropy of the exchange coupling.

Results for 2. For **2**, the model system comprises an exchange-coupled tetramer $W^V{-}Ce^{III}{-}Ce^{III}{-}W^V$, which corresponds exactly to the structural data. The coupling constant J_{CeCe} was fixed at the value of -1.1 cm^{-1} obtained for **1** because the Ce ions in the tetramer are linked through the same bridging ligand. The best fit to the experimental data was found for the following set of parameters: $g_{Ce} = 0.92(1)$, $J_{CeW} = 1.7(2)$, $A_2^0\langle r^2\rangle = -848(8)$, $A_4^0\langle r^4\rangle = -276(45)$, and $A_4^3\langle r^4\rangle = -1050(7)$. As can be seen from Figure 5, the best-fit curves (solid lines) satisfactorily reproduce the experimental data. The lowest sublevel for an isolated Ce^{III} ion in **2** is a Kramers doublet comprising a superposition of the $|\pm^1/_2\rangle$ and $|\pm^5/_2\rangle$ substates (Table S3 in the Supporting Information), with the dominant contribution from the former substates. The first excited-state Kramers doublet corresponds to the $|\pm^3/_2\rangle$ substates, whereas the highest-lying Kramers doublet is again a superposition of the $|\pm^1/_2\rangle$ and $|\pm^5/_2\rangle$ substates, with the dominant contribution from the substates with the highest $|J_z|$ value. At $T = 2$ K, the population of the ground-state level is practically 100%. It is only at $T = 100$ K that the population of the first excited-state Kramers doublet (1.8%) stops being negligible. The populations for the successive Kramers doublets at $T = 200$ K amount to 87%, 11.7%, and 1.3%, respectively. The above facts account for the monotonic decrease of the χT values upon lowering temperature. The exchange coupling between either W^V and Ce^{III} ions or Ce^{III} and Ce^{III} ions is accountable for the downturn of the χT curve observed at low temperatures. Because the lowest-lying Kramers doublet is well separated from the excited ones, the system can be at low temperatures described by an effective exchange Hamiltonian

$$H_{EFF2} = -\tilde{S}_{Ce1}\cdot\mathbf{J}_{CeW1}\cdot\mathbf{S}_{W1} - \tilde{S}_{Ce2}\cdot\mathbf{J}_{CeW2}\cdot\mathbf{S}_{W2} - \tilde{S}_{Ce1}\cdot\mathbf{J}_{CeCe}\cdot\tilde{S}_{Ce2}$$

where $\mathbf{J}_{CeCe}$, $\mathbf{J}_{CeW1}$, and $\mathbf{J}_{CeW2}$ are symmetric exchange-coupling matrices and $\tilde{S}_{Ce1}$ and $\tilde{S}_{Ce2}$ denote the effective spin operators corresponding to the lowest doublet.

Analogous interpretation as for **1** leads to the conclusion that exchange-coupling matrices $\mathbf{J}_{CeCe}$, $\mathbf{J}_{CeW1}$, and $\mathbf{J}_{CeW2}$ are diagonal in the coordinate frame, where the corresponding spectroscopic tensor of the cerium center is diagonal with the principal values equal respectively to $J_{CeCei} = (g_{Ce} - 1)^2(g_{Ceii}/g_{Ce})^2 J_{CeCe}$ and $J_{CeWi} = (g_{Ce} - 1)(g_{Ceii}/g_{Ce})\, J_{CeW}$ ($i = x, y, z$). Decomposition of the exchange-coupling matrices into isotropic and anisotropic parts and use of the best-fit values of the corresponding parameters yield the following estimates: $J_{iso} = -0.123$, $D_{xx} = D_{yy} = -0.06$, and $D_{zz} = 0.121$ for Ce−Ce coupling and $J_{iso} = -0.489$, $D_{xx} = D_{yy} = -0.205$, and $D_{zz} = 0.410$ (in cm^{-1}) for Ce−W coupling. The ratios $J_{CeCez}/J_{CeCex(y)} = 0.02$ and $J_{CeWz}/J_{CeWx(y)} = 0.11$ indicate again the XXZ exchange anisotropy. The difference in the signs of J_{iso} and J_{CeW} stems from the fact that the effective spin of the Ce^{III} center is parallel to its total angular momentum J_{Ce} but antiparallel to its spin angular momentum.

Results for 3. Because there is no strict model system to account for the 2D topology of magnetic couplings in **3**, we introduce a necessary simplified two-step approach. The result obtained for **1** implies that the expected energy scale of the exchange interaction between the Ce^{III} ions mediated through bpm ligands is relatively low. Weak antiferromagnetic coupling (≈ -0.02 cm^{-1}) mediated through the bpm ligand was also found in $[Gd(L^2)_3]_2(\mu\text{-bpm})$ (L^2 = dimethyl-*N*-trichloroacetylamidophosphate).[22] A higher value of the exchange coupling (≈ -1.2 cm^{-1}) across the bis-chelating bpm ligand was reported between the Mn^{II} ions in $(\mu\text{-bpm})[Mn(H_2O)_3\{Fe(bipy)(CN)_4\}]_2[Fe(bipy)(CN)_4]_2 \cdot 12H_2O$ (bipy−bipyridine)[70] or between Mn^{III} and Cr^{III} (≈ -2.0 cm^{-1}) in $[Mn^{III}(salhd)(\mu\text{-}CN)Cr^{III}(CN)_3(bpm)(H_2O)_2]_n$.[71] At the same time, the coupling between W^V and Ce^{III} ions through the CN^- bridges is expected to be more efficient. Moreover, it is expected that the exchange couplings involved are at least 1 order of magnitude smaller than the LF parameters, so neglecting one of them shall not lead to substantial changes in the LF. Therefore, we assume that neglecting the exchange interaction between the cerium centers will yield an acceptable approximation for the LF. Then our system simplifies to that of alternating chains of W^V and Ce^{III} centers. The corresponding exchange Hamiltonian reads

$$H_{EX} = -\sum_{i=1}^{n} J_{CeW}(g_J - 1)\mathbf{J}_{Cei} \cdot (\mathbf{S}_{Wi} + \mathbf{S}_{Wi+1})$$

We further choose to use a short-chain model comprising only two W^V ions and two Ce^{III} ions with imposed periodic boundary conditions, i.e., $\mathbf{S}_{Wn+1} = \mathbf{S}_{W1}$. With these approximating assumptions, the value of the exchange coupling constant J_{CeW} obtained from the fit will set an upper bound on the genuine value. The best fit was obtained for $g_{Ce} = 0.82(1)$, $J_{CeW} = 6.7(1)$, $A_2^0\langle r^2\rangle = -777(39)$, $A_4^0\langle r^4\rangle = -374(57)$, and $A_4^3\langle r^4\rangle = -414(17)$. In Figure 6, the best-fit curves (solid lines) of the susceptibility and isothermal magnetization are shown. The lowest Kramers doublet of the ground-state multiplet is a superposition of $|\pm^1/_2\rangle$ and $|\pm^5/_2\rangle$ substates, with the dominant contribution (97.1%) from substates with the lowest $|J_z|$ value (Table S4 in the Supporting InFormation). At $T = 2$ K, the population of the ground state is almost 100%, and it decreases only to 96.5% at $T = 100$ K, whereas the first excited-state Kramers doublet comprising the $|\pm^3/_2\rangle$ substates becomes populated to 3.3%. The population of the second excited-state Kramers doublet corresponding to the highest $|J_z|$ values amounts merely to 0.2%. Those facts explain the relatively rapid decrease of the χT product upon lowering temperature. The sudden drop of the χT values below 6 K is ascribed to the onset of the exchange coupling between the W^V and Ce^{III} ions. In order to estimate the initially neglected Ce−Ce exchange coupling, we performed the calculations for an eight-center grid (Scheme 2), confining the space of the states of the Ce ions to the lowest Kramers doublet (Table S4 in the Supporting Information). Only isotropic coupling between the magnetic centers was assumed because the extension to anisotropic terms led to uncontrolled overparametrization. Figure 6 shows the results of the calculations (red dashed lines) obtained with $J_{CeCe} = -0.5(2)$ cm^{-1} and $J_{CeW} = 1.4(3)$ cm^{-1}. Similar to **1** and **2**, the Ce−Ce exchange interaction is of antiferromagnetic character and the Ce−W interaction is ferromagnetic.

Scheme 2. Eight-Center Grid Used To Estimate the Exchange Couplings in **3**[a]

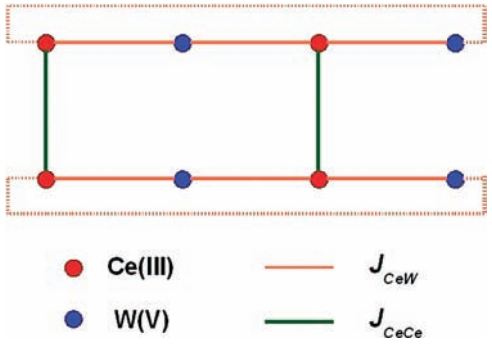

[a] Dotted lines indicate the periodic boundary conditions imposed on the grid.

Application of the generalized van Vleck formalism enabled estimation of the LF parameters for the Ce^{III} ions and determination of the exchange couplings between the constituent magnetic ions in **1**−**3**. The proximity of the coordination geometry of the Ce^{III} ions to a distorted TTP resulted in the same set of LF parameters, yielding the best fit. In particular, compounds **1** and **2** display considerable similarity in the Kramers doublet spectrum, which indicates the proximity of their LF configurations. The exchange coupling mediated through the bpm ligand was found to be rather weak and antiferromagnetic ($J_{CeCe} = -1.1(1)$ cm^{-1} in **1** and $-0.5(2)$ in **3**), whereas the coupling between the Ce^{III} and W^V ions linked by the cyanide bridge turned out to be more effective and ferromagnetic. For **2**, the value of J_{CeW} amounts to 1.7(2) cm^{-1}, whereas for **3**, the value estimated on the basis of the eight-center-grid model is 1.4(3) cm^{-1}, which is consistent with the preliminary upper bound of 6.7(1) cm^{-1}. The calculations imply an XXZ anisotropy of exchange interactions in the

(70) Toma, L. M.; Lescouëzec, R.; Toma, L. D.; Lloret, F.; Julve, M.; Vaissermann, J.; Andruh, M. *J. Chem. Soc., Dalton Trans.* **2002**, 3171.
(71) Visinescu, D.; Toma, L. M.; Lloret, F.; Fabelo, O.; Ruiz-Pérez, C.; Julve, M. *Dalton Trans.* **2008**, 4103.

ground state. Such an anisotropy was predicted theoretically for the $Yb^{III}-Cr^{III}$ exchange-coupled dimer, where the electronic configuration of Yb^{III} ($4f^{13}$) is complementary to that of Ce^{III} ($4f^{1}$).[72]

In conclusion, we have shown that assembling Ce^{3+}, $[W(CN)_8]^{3-}$, and bpm linker in different experimental conditions is an efficient route toward magnetic {4f−5d} inorganic−organic hybrid materials via secondary building block {Ce−bpm−Ce}. The magnetostructural correlation for **1**−**3** enabled estimation of the LF parameters for the Ce^{3+} ions and determination of the exchange couplings for {Ce−NC−W} and {Ce−bpm−Ce} linkages.

The rather weak and antiferromagnetic (J_{CeCe} = $-1.1(1)$ cm^{-1}) exchange coupling mediated through the bpm ligand can be compared to the more effective and ferromagnetic coupling between the Ce^{III} and W^{V} ions linked by the cyanide bridge [J_{CeW} = 1.7(2) (**2**) and 1.4(3) cm^{-1} (**3**)]. However, no clear correlation between the magnitude of J_{CeW} and the structural parameters of the {Ce−NC−W} linkage can be obtained. In order to find the relationship between the magnitude of J_{LnW} and the structural parameters of the {Ln−NC−W} linkage, further investigations on materials based on other Ln^{3+} cations and $[W(CN)_8]^{3-}$ with the bpm linker are currently in progress.

Acknowledgment. This work was supported by the Polish Ministry of Science and Higher Education within Research Project 3327/B/H03/2009/37.

Supporting Information Available: Crystallographic information files (CIF) for compounds **1**−**3**, graphical representation of asymmetric units for **2** and **3** and coordination spheres of cerium in **1**−**3**, and experimental results including TGA for **1**−**3**, an extended operator equivalents table, and characterization of the Kramers doublets for **1**−**3**. This material is available free of charge via the Internet at http://pubs.acs.org.

(72) Mironov, V. S.; Chibotaru, L. F.; Ceulemans, A. *Phys. Rev.* **2003**, *B 67*, 014424.